# Ultrasmall subwavelength nanorod plasmonic cavity

**Ju-Hyung Kang,[1] You-Shin No,[1] Soon-Hong Kwon,[2,3] and Hong-Gyu Park[1,*]**

[1]*Department of Physics, Korea University, Seoul 136-701, South Korea*

[2]*Department of Physics, Chung-Ang University, Seoul 156-756, South Korea*

[3]*e-mail: soonhong.kwon@gmail.com*

**Corresponding author: hgpark@korea.ac.kr*

Received March 8, 2011; revised April 22, 2011; accepted April 22, 2011;
posted April 25, 2011 (Doc. ID 143598); published May 26, 2011

We propose an ultrasmall plasmonic cavity consisting of a high-index/low-index dielectric nanorod covered with silver. Full three-dimensional subwavelength confinement of the surface-plasmon polaritons was achieved at the high-index dielectric–silver interface without propagating to the low-index dielectric–silver interface. The numerical simulations showed that the plasmonic mode excited in this cavity has a deep subwavelength mode volume of $0.0038(\lambda/2n)^3$ and a quality factor of 1500 at 40 K, and consequently a large Purcell factor of $\sim 2 \times 10^5$. Therefore, this plasmonic cavity is expected to be useful for the demonstration of high-efficiency single photon sources or low-threshold lasers in an ultracompact nanophotonic circuit. © 2011 Optical Society of America

*OCIS codes:* 220.4241, 250.5403, 310.6628.

Ultrasmall cavities enable the demonstration of high-performance photonic devices, such as low-threshold lasers [1] and high-efficiency single photon sources [2,3]. Plasmonic cavities are particularly attractive because they can support resonant modes with a subwavelength mode volume in contrast to dielectric cavities [4–10]. Although small mode volumes were achieved in metal-coated dielectric cavities, further miniaturization is restricted by the diffraction limit [11–13]. Recently, several plasmonic cavities were proposed and plasmonic lasing was also demonstrated using some of them [8–10]. However, further reduction in the mode volume in a plasmonic cavity is still necessary for the miniaturization and high-density integration of plasmonic devices. In this Letter, we show that the ratio between quality ($Q$) factor and mode volume ($V$), $Q/V$, can be increased significantly through rational design of a plasmonic cavity. The numerical simulation demonstrates that the mode volume can be reduced to $0.0038(\lambda/2n)^3$, which is two or three orders of magnitude smaller than the mode volumes of conventional dielectric cavities [1,14] and ten times smaller than the volumes of the previous smallest plasmonic cavities [4–6]. In particular, the large Purcell factor obtained in this cavity, $\sim 2 \times 10^5$, enables the demonstration of high-efficiency single photon sources [2,3], ultrafast lasers [15], and low-threshold lasers [1,14].

Figure 1(a) shows a schematic diagram of the plasmonic cavity, a dielectric nanorod with a rectangular cross section that is covered with silver. The nanorod on a transparent sapphire substrate consists of high- and low-index dielectric materials with heights of $L_c$ and $L_m$, respectively. The surface-plasmon polaritons (SPPs) can then be confined strongly only at the high-index dielectric–silver interface due to the large frequency gap between the SPP mode excited at the high-index dielectric–silver interface and the one at the low-index dielectric–silver interface [6]. Furthermore, since the top of the nanorod is covered with silver, a subwavelength plasmonic cavity mode is formed, showing an extremely small mode volume. In addition, the SPPs can be excited efficiently at the nanorod–silver interface by optical pumping through the transparent bottom sapphire substrate [8].

To understand quantitatively the confinement mechanism of the SPPs in this cavity, we calculated dispersion curves of the fundamental SPP waveguide modes in rectangular cross-sectional dielectric waveguides covered by silver [Fig. 1(b)]. Two different dielectric cores with refractive indices ($n$) of 3.4 (circles; e.g., InP or GaAs) and 1.5 (squares) were used. Silver was modeled by the Drude model: $\varepsilon(\omega) = \varepsilon_\infty - \omega_p^2/(\omega^2 + i\gamma\omega)$, which is fitted by the experimentally determined dielectric function of silver [16]. The background dielectric constant $\varepsilon_\infty$, the plasma frequency $\omega_p$, and the collision frequency $\gamma$ at room temperature were 3.1, $1.4 \times 10^{16}\ \mathrm{s}^{-1}$, and $3.1 \times 10^{13}\ \mathrm{s}^{-1}$, respectively [8]. The finite-difference time-domain (FDTD) simulation with a spatial resolution of 1 nm was used for these calculations. The sides of the waveguide cross section were set to be $w = 200$ nm and $d = 100$ nm, respectively. We note that such two-dimensional dielectric

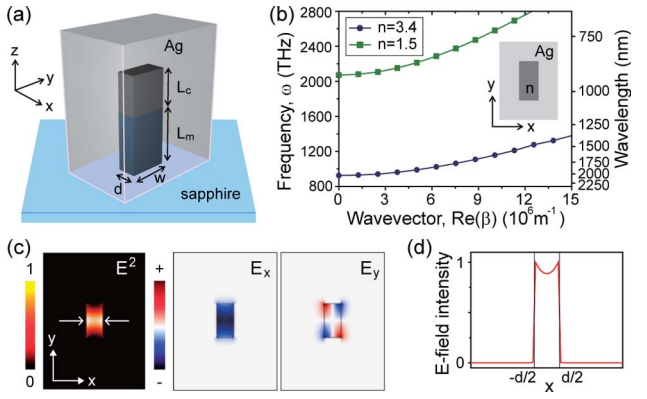


Fig. 1. (Color online) (a) Schematic diagram of the SPP cavity consisting of a high-index (dark gray, top)/low-index (blue, bottom) dielectric nanorod covered by silver. The cavity was placed on a sapphire substrate. (b) Calculated dispersion curves of the fundamental SPP mode for the core refractive indices of 3.4 (circles) and 1.5 (squares). We set $w = 200$ nm and $d = 100$ nm. The inset shows a cross-sectional view of the waveguide. (c) Electric field profiles ($E^2$, $E_x$, $E_y$) of the fundamental SPP mode for the high-index dielectric core–silver shell waveguide. (d) Electric field intensity distribution calculated along the arrows in (c).

 © 2011 Optical Society of America

core–metal shell waveguides have cutoff frequencies at a zero wave vector in contrast to conventional one-dimensional metal–insulator–metal structures [6,17]. The cutoff frequency depends on the refractive index of the dielectric core of the waveguide, $n$: a smaller $n$ provides a larger cutoff frequency [6]. Figure 1(b) shows that the cutoff frequencies vary from 926 to 2072 THz by changing $n$ from 3.4 to 1.5. In addition, the cutoff frequencies can be controlled depending on the structural parameters of the waveguides, such as $w$ and $d$.

The electric field profiles ($E^2$, $E_x$, $E_y$) of the fundamental SPP waveguide mode were also calculated at $w = 200\,\text{nm}$, $d = 100\,\text{nm}$, and $n = 3.4$ [Fig. 1(c)]. The FDTD simulation of the electric field intensity profile, $E^2$, shows that the SPPs are strongly confined at the dielectric–silver interface. The cross-sectional view of the electric field intensity along the $x$ axis at the center of waveguide clarifies this key feature of the SPP mode with an intensity maximum at the interface [Fig. 1(d)] [18]. Furthermore, the electric field direction is normal to the dielectric–silver interface, as shown in the electric field patterns of $E_x$ and $E_y$ [middle and right panels, Fig. 1(c)].

A three-dimensional FDTD simulation was performed to examine the confinement of the SPPs in the nanorod SPP cavity consisting of two stacked dielectric core–silver shell waveguides with different core materials, high- and low-index dielectric materials (Fig. 2). A dipole emitter was used to excite an SPP mode, which was 1 nm away from the sidewall of the silver surface. The simulation shows that the SPPs are strongly confined at the high-index dielectric–silver interface as expected [Fig. 2(a)]. In this simulation, the following structural parameters were used: $w = 200\,\text{nm}$, $d = 100\,\text{nm}$, $L_c = 200\,\text{nm}$, and $L_m = 300\,\text{nm}$. Indeed, the SPPs are confined in this cavity by two mechanisms, the metal reflection (upper end of the high-index dielectric) and the frequency mode gap [6] (lower end of the high-index dielectric). The novel confinement process by the frequency mode gap can be understood from the band diagram of the fundamental SPP mode [Fig. 2(b)]. If the mode frequency of interest ($\omega$) is between the cutoff frequencies of the high-index dielectric–silver waveguide ($\omega_{\text{high}}$) and low-index dielectric–silver waveguide ($\omega_{\text{low}}$), the SPP mode can be confined to the high-index dielectric–silver interface without propagating to the low-index dielectric–silver interface. Furthermore, since the bottom of the nanorod is open and uncovered by silver, this mode-gap confinement, which is widely used in dielectric cavities [19], enables efficient light excitation and collection through the transparent sapphire substrate as well as deep subwavelength SPP confinement.

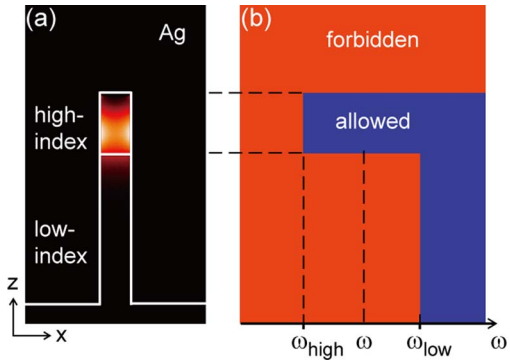


Fig. 2. (Color online) (a) Electric field intensity profile of the SPP mode excited in the high-index/low-index dielectric nanorod SPP cavity. $L_c = 200\,\text{nm}$, $w = 200\,\text{nm}$, and $d = 100\,\text{nm}$. (b) Band diagram of the SPP mode corresponding to (a). Allowed and forbidden regions are drawn along the $z$ axis.

Systematic FDTD simulations were performed with various structural parameters of the nanorod SPP cavity to examine the optical properties. First, the cutoff frequencies of the high-index dielectric–silver waveguide modes were calculated as a function of $w$ and $d$ [Fig. 3(a)]. These simulation results can be obtained using the periodic boundary conditions along the propagation direction at a zero wave vector. In this color map, red (top left) and violet (bottom right) indicate higher and lower frequencies, respectively. This map can be used to estimate the resonant frequency of the SPP cavity mode, as shown in Fig. 2(a), because the frequency of the cavity mode will be slightly larger than the cutoff frequency. For example, if one is interested in a cavity mode with a resonant frequency of 1550 nm, the simulations can be carried out using particular sets of $w$ and $d$ corresponding to the black dots in Fig. 3(a), where the cutoff frequencies are 1550 nm. Indeed, the calculated resonant frequencies of the cavity modes with those parameter sets are all approximately 1550 nm with an error of tens of nanometers.

Next, a nanorod SPP cavity with $L_c = 200\,\text{nm}$ was defined, and the $Q$ factors at 40 K and mode volumes were calculated as a function of the cross-sectional area of the cavity, $w$ times $d$ [Fig. 3(b)]. The $Q$ factor was calculated from the time decay of the energy of a cavity mode. The mode volume was defined as the ratio of the total electric field energy density of the mode to the peak energy density, where the effective refractive index of metal was used [4,6,8]. To present the ohmic losses of silver at low temperature, the damping collision frequency, $\gamma$,

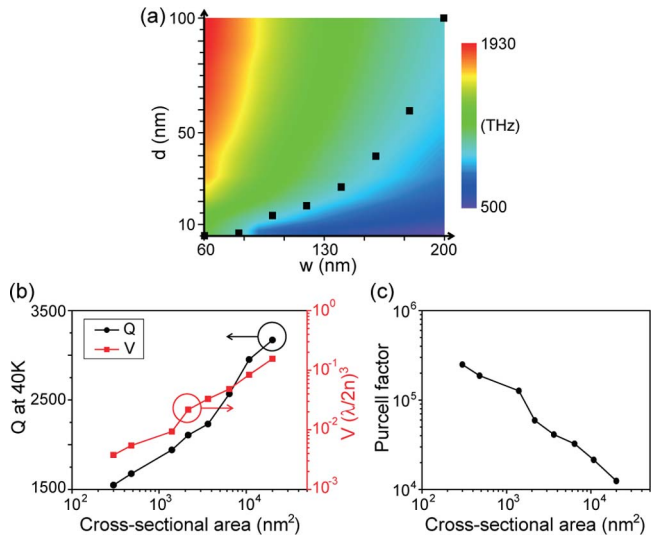


Fig. 3. (Color online) (a) Cutoff frequency color map calculated as a function of $w$ and $d$ in the high-index dielectric core–silver shell SPP waveguide. The cutoff frequency decreases with increasing $w$ and decreasing $d$. (b) $Q$ factors at 40 K (circles) and mode volumes (squares) calculated as a function of the cross-sectional area, $w$ times $d$. ($w$, $d$) varies from (200 nm, 100 nm) to (60 nm, 5 nm). (c) Purcell factor calculated as a function of the cross-sectional area.

was scaled by a factor of the room-temperature conductivity of a metal divided by the conductivity at 40 K [6,8,10,11]. The $Q$ factor at 40 K suggests the lower limit for the solid-state cavity quantum electrodynamics (QED) experiments such as single photon source and strong coupling whose operational temperature usually ranges from 0 to 40 K [2–4].

The structural parameters of the black dots in Fig. 3(a), $w$ and $d$, were used so that the resonant wavelengths of the cavity would all be approximately 1550 nm. The FDTD simulation shows that the mode volumes (squares) decrease significantly from 0.15 to $0.0038(\lambda/2n)^3$ with decreasing cross-sectional area from $2 \times 10^4$ to $3 \times 10^2$ nm$^2$, whereas the $Q$ factors (circles) decrease slightly from 3200 to 1500. It is notable that the mode volumes decrease much faster than $Q$ factors with shrinking physical cavity size. As a result, an extremely small mode volume of $0.0038(\lambda/2n)^3$ was obtained. On the other hand, the $Q$ factors decrease due to the increased overlap of the electric fields with the metal so the mode will show increased metallic absorption loss.

One can expect that the nanorod SPP cavities can have large Purcell factors because the mode volumes of these cavities are extremely small. In Fig. 3(c), the Purcell factors, $F$, were calculated as a function of the cross-sectional area using the following equation [2]:

$$F = \frac{3}{4\pi^2}\left(\frac{\lambda}{n}\right)^3\left(\frac{Q}{V}\right), \tag{1}$$

where the $Q$ factors and mode volumes of Fig. 3(b) were used. An emitter was assumed to be placed at the modal field maximum to calculate the maximum enhancement of Purcell factor. Consequently, a large Purcell factor $> \sim 2 \times 10^5$ was obtained at a cavity of 60 nm × 5 nm × 200 nm [Fig. 3(c)]. Hence, spontaneous emission from this cavity can be enhanced considerably due to this large Purcell factor. Even if a tenfold drop in $Q$ factor is considered at room temperature, the Purcell factor is still large, $\sim 2 \times 10^4$, owing to the ultrasmall mode volume of $0.0038(\lambda/2n)^3$. A large average Purcell factor [20] was also calculated, $\sim 9.3 \times 10^4$. Moreover, when a gain material, e.g., quantum wells, has a larger linewidth due to homogeneous broadening than the cavity linewidth, the Purcell factor in the above equation is limited by emitter $Q$ factor, $Q_{\text{emit}}$ (10–100), not cavity $Q$ factor, $Q_{\text{cav}}$ [21]. Therefore, when $Q_{\text{cav}}$ is larger than $Q_{\text{emit}}$, the Purcell factor is enhanced more effectively by reducing the mode volume, which is the most attractive feature of the SPP cavity. Our SPP cavity with a large Purcell factor and ultrasmall mode volume is a strong candidate for high-efficiency single-photon sources, low-threshold lasers, and ultrafast lasers using quantum wells or quantum dots.

In summary, this study proposes a novel ultrasmall subwavelength SPP cavity consisting of a high-index/low-index dielectric nanorod covered by silver. The $Q$ factors and mode volumes were calculated. The FDTD simulation showed that the ultrasmall mode volume of $0.0038(\lambda/2n)^3$ yielded a large Purcell factor $> \sim 2 \times 10^5$ at 40 K. Enhanced spontaneous emission due to such a large Purcell factor can result in high-performance nanophotonic devices, particularly a high-efficiency single-photon source. An understanding of the strong confinement of the SPPs in a subwavelength volume will also be useful in solid-state cavity QED experiments based on the GaAs material system [2,3].

This work was supported by Creative Research Initiatives (grant 2011-0000419) of the Ministry of Education, Science, and Technology (MEST)/Korea Science and Engineering Foundation (KOSEF). Y.-S. No acknowledges the support of this work by the TJ Park Doctoral Fellowship.

**References**

1. H.-G. Park, S.-H. Kim, S.-H. Kwon, Y.-G. Ju, J.-K. Yang, J.-H. Baek, S.-B. Kim, and Y.-H. Lee, Science **305**, 1444 (2004).
2. D. Englund, D. Fattal, E. Waks, B. Zhang, T. Nakaoka, Y. Arakawa, Y. Yamamoto, and J. Vuckovic, Phys. Rev. Lett. **95**, 013904 (2005).
3. J. P. Reithmaier, G. Sek, A. Loffler, C. Hofmann, S. Kuhn, S. Reitzenstein, L. V. Keldysh, V. D. Kulakovskii, T. L. Reinecke, and A. Forchel, Nature **432**, 197 (2004).
4. Y. Gong and J. Vuckovic, Appl. Phys. Lett. **90**, 033113 (2007).
5. M. Kuttge, F. J. Garcia de Abajo, and A. Polman, Nano Lett. **10**, 1537 (2010).
6. M.-K. Seo, S.-H. Kwon, H.-S. Ee, and H.-G. Park, Nano Lett. **9**, 4078 (2009).
7. B. Min, E. Ostby, V. Sorger, E. Ulin-Avila, L. Yang, X. Zhang, and K. Vahala, Nature **457**, 455 (2009).
8. S.-H. Kwon, J.-H. Kang, C. Seassal, S.-K. Kim, P. Regreny, Y.-H. Lee, C. M. Lieber, and H.-G. Park, Nano Lett. **10**, 3679 (2010).
9. R. F. Oulton, V. J. Sorger, T. Zentgraf, R. M. Ma, C. Gladden, L. Dai, G. Bartal, and X. Zhang, Nature **461**, 629 (2009).
10. M. T. Hill, M. Marell, E. S. P. Leong, B. Smalbrugge, Y. Zhu, M. Sun, P. J. van Veldhoven, E. J. Geluk, F. Karouta, Y. Oei, R. Notzel, C. Z. Ning, and M. K. Smit, Opt. Express **17**, 11107 (2009).
11. M. T. Hill, Y.-S. Oei, B. Smalbrugge, Y. Zhu, T. de Vries, P. J. van Veldhoven, F. W. M. van Otten, T. J. Eijkemans, J. P. Turkiewicz, H. de Waardt, E. J. Geluk, S.-H. Kwon, Y.-H. Lee, R. Notzel, and M. K. Smit, Nat. Photon. **1**, 589 (2007).
12. M. P. Nezhad, A. Simic, O. Bondarenko, B. Slutsky, A. Mizrahi, L. Feng, V. Lomakin, and Y. Fainman, Nat. Photon. **4**, 395 (2010).
13. I. S. Maksymov, M. Besbes, J. P. Hugonin, J. Yang, A. Beveratos, I. Sagnes, I. Robert-Philip, and P. Lalanne, Phys. Rev. Lett. **105**, 180502 (2010).
14. K. Nozaki and T. Baba, Appl. Phys. Lett. **88**, 211101 (2006).
15. D. Englund, H. Altug, B. Ellis, and J. Vuckovic, Laser Photon. Rev. **2**, 264 (2008).
16. P. B. Johnson and R. W. Christy, Phys. Rev. B **6**, 4370 (1972).
17. J. A. Dionne, H. J. Lezec, and H. A. Atwater, Nano Lett. **6**, 1928 (2006).
18. S. A. Maier, *Plasmonics: Fundamentals and Applications* (Springer, 2007).
19. K. Srinivasan and O. Painter, Opt. Express **10**, 670 (2002).
20. M. Makarova, V. Sih, J. Warga, R. Li, L. D. Negro, and J. Vuckovic, Appl. Phys. Lett. **92**, 161107 (2008).
21. K. Nozaki, S. Kita, and T. Baba, Opt. Express **15**, 7506 (2007).